Thermal imaging of a heat transport in regions structured by femtosecond laser

Junko Morikawa,[1,*] **Eita Hayakawa,**[2] **Toshimasa Hashimoto,**[1]
Ričardas Buividas,[3] **Saulius Juodkazis**[3,4]

[1] *Tokyo Institute of Technology, Meguro-ku, Tokyo 152-8550, Japan*
[2] *ai-Phase, Co., Ltd., Shinagawa-ku, Tokyo 141-0021, Japan*
[3] *Centre for Micro-Photonics, Faculty of Engineering and Industrial Sciences, Swinburne University of Technology, Hawthorn, VIC 3122, Australia*
[4] *Melbourne Centre for Nanofabrication, 151 Wellington Road, Clayton, VIC 3168, Australia*
[*] *morikawa.j.aa@m.titech.ac.jp*

Abstract: A non-contact determination of thermal diffusivity and spatial distribution of temperature on tens-of-micrometers scale is demonstrated by thermal imaging. Temperature localization and a heat flow have been *in situ* monitored with ~ 10 ms temporal resolution in Kapton polymer films structured by femtosecond laser pulses. The structured regions can localize temperature and create strong thermal gradients of few degrees over tens-of-micrometers (~ 0.1 K/μm). This is used to induce an anisotropy in a heat transport. Temperature changes on the order of $\sim 0.1^{\circ}$C were reliably detected and spatial spreading by diffusion was monitored using Fourier analysis. Application potential, miniaturization prospects, and emissivity changes induced by laser structuring of materials are discussed.

OCIS codes: (110.6820) Thermal imaging; (140.3390) Laser material processing; (160.5470) Polymers; (350.3850) Materials processing; (160.1245) Artificially engineered materials; (110.3080) IR imaging.

References and links

1. T. Baldacchini, C. N. LaFratta, R. A. Farrer, M. C. Teich, B. E. A. Saleh, M. J. Naughton, and J. T. Fourkas, "Acrylic-based resin with favorable properties for three-dimensional two-photon polymerization," J. Appl. Phys. **95**, 6072–6076 (2004).
2. M. Ams, G. D. Marshall, P. Dekker, J. A. Piper, and M. J. Withford, "Ultrafast laser written active devices," Laser Photon. Rev. **3**, 535–544 (2009).
3. S. Maruo, O. Nakamura, and S. Kawata, "Three-dimensional microfabrication with two-photon-absorbed photopolymerization," Opt. Lett. **2**, 132 – 134 (1997).
4. S. Maruo and K. Ikuta, "Three-dimensional microfabrication by use of single-photon-absorbed polymerization," Appl. Phys. Lett. **76**, 2656–2658 (2000).
5. S. Kawata, H.-B. Sun, T. Tanaka, and K. Takada, "Finer features for functional microdevices," Nature **412**, 697–698 (2001).
6. O. Breitenstein, J. Bauer, K. Bothe, W. Kwapil, D. Lausch, U. Rau, J. Schmidt, M. Schneemann, M. C. Schubert, J.-M. Wagner, and W. Warta, "Understanding junction breakdown in multicrystalline solar cells," J. Appl. Phys. **109**, 071101 (2011).
7. K. Juodkazis, J. Juodkazytė, P. Kalinauskas, E. Jelmakas, and S. Juodkazis, "Photoelectrolysis of water: Solar hydrogen - achievements and perspectives," Opt. Express: energy express **18**, A147–A160 (2010).
8. M. Schmotz, P. Bookjans, E. Scheer, and P. Leiderer, "Optical temperature measurements on thin freestanding silicon membranes," Rev. Sci. Instrum. **81**, 114903 (2010).
9. W. Gawelda, D. Puerto, J. Siegel, A. Ferrer, A. R. de la Cruz, H. Fernandez, and J. Solis, "Ultrafast imaging of transient electronic plasmas produced in conditions of femtosecond waveguide writing in dielectrics," Appl. Phys. Lett. **93**, 121109/1–3 (2008).

#151731 - $15.00 USD Received 25 Jul 2011; revised 5 Sep 2011; accepted 5 Sep 2011; published 3 Oct 2011

10. Y. Bellouard, M. Dugan, A. A. Said, and P. Bado, "Thermal conductivity contrast measurement of fused silica exposed to low-energy femtosecond laser pulses," Appl. Phys. Lett. **89**, 161911 (2006).
11. J. Morikawa, A. Orie, T. Hashimoto, and S. Juodkazis, "Thermal diffusivity in femtosecond-laser-structured micro-volumes of polymers," Appl. Phys. A. **98**(3), 551–556 (2010).
12. J. Morikawa, A. Orie, T. Hashimoto, and S. Juodkazis, "Thermal and optical properties of femtosecond laser-structured PMMA," Appl. Phys. A **101**, 27–31 (2010).
13. J. Morikawa, A. Orie, T. Hashimoto, and S. Juodkazis, "Thermal and optical properties of the femtosecond-laser-structured and stress-induced birefringent regions of sapphire," Opt. Express **18**, 8300–8310 (2010).
14. M. Farsari and B. Chichkov, "Materials processing: Two-photon fabrication," Nature Photonics **3**, 450 – 452 (2009).
15. K. K. Seet, S. Juodkazis, V. Jarutis, and H. Misawa, "Feature-size reduction of photopolymerized structures by femtosecond optical curing of SU-8," Appl. Phys. Lett. **89**, 024106 (2006).
16. L. Hallo, C. Mézel, A. Bourgeade, D. Hébert, E. G. Gamaly, and S. Juodkazis, *Laser-Matter Interaction in Transparent Materials: Confined Micro-explosion and Jet Formation*, 121–146. NATO Science for Peace and Security Series B: Physics and Biophysics, Springer Netherlands, 2009.
17. T. Kudrius, G. Šlekys, and S. Juodkazis, "Surface-texturing of sapphire by femtosecond laser pulses for photonic applications," J. Phys. D: Appl. Phys. **43**, 145501 (2010).
18. L. Bressel, D. de Ligny, C. Sonneville, V. Martinez-Andrieux, V. Mizeikis, R. Buividas, and S. Juodkazis, "Femtosecond laser induced density changes in GeO_2 and SiO_2 glasses: fictive temperature effect," Opt. Mater. Express **1**, 605–613 (2011).
19. G. Cerullo, R. Osellame, S. Taccheo, M. Marangoni, D. Polli, R. Ramponi, P. Laporta, and S. D. Silvestri, "Femtosecond micromachining of symmetric waveguides at 1.5μm by astigmatic beam focusing," Opt. Lett. **27**, 1938–1940 (2002).
20. G. Cheng, K. Mishchik, C. Mauclair, E. Audouard, and R. Stoian, "Ultrafast laser photoinscription of polarization sensitive devices in bulk silica glass," Opt. Express **17**, 9515–9525 (2009).
21. D. Day and M. Gu, "Microchannel fabrication in PMMA based on localized heating by nanojoule high repetition rate femtosecond pulses," Opt. Express **13**, 5939–5946 (2005).
22. S. Nolte, M. Will, J. Burghoff, and A. Tünnermann, "Femtosecond waveguide writing: a new avenue to three-dimensional integrated optics," Appl. Phys. A **77**, 109–111 (2003).
23. L. Shah, A. Arai, S. Eaton, and P. Herman, "Waveguide writing in fused silica with a femtosecond fiber laser at 522 nm and 1 MHz repetition rate," Opt. Express **13**, 1999–2006 (2005).
24. J. Wu and X. Gan, "Three dimensional nanoparticle trapping enhanced by surface plasmon resonance," Opt. Express **18**, 27619–27626 (2010).
25. H. Misawa and S. Juodkazis, "Photophysics and photochemistry of a laser manipulated microparticle," Prog. Polym. Sci. **24**, 665–697 (1999).
26. E. Brasselet and S. Juodkazis, "Optical angular manipulation of liquid crystal droplets in laser tweezers," J. of Nonlin. Opt. Phys. and Mat. **18**, 167–194 (2009).
27. O. A. Louchev, S. Juodkazis, N. Murazawa, S. Wada, and H. Misawa, "Coupled laser molecular trapping, cluster assembly, and deposition fed by laser-induced Marangoni convection," Opt. Express **16**, 5673–5680 (2008).
28. A. I. Hochbaum, R. Chen, R. D. Delgado, W. Liang, E. C. Garnett, M. Najarian, A. Majumdar, and P. Yang, "Enhanced thermoelectric performance of rough silicon nanowires," Nature **451**, 163 – 167 (2008).
29. J. Morikawa, A. Orie, Y. Hikima, T. Hashimoto, and S. Juodkazis, "Influence of ordering change on the optical and thermal properties of inflation polyethylene films," Appl. Surf. Sci. **257**, 5439–5442 (2011).
30. Y. Gu, X. Tang, Y. Xu, and I. Hatta, "Ingenious method for eliminating effects of heat loss in measurements of thermal diffusivity by ac calorimetric method," Jpn. J. Appl. Phys. **32**, L1365 – L1367 (1993).
31. J. Morikawa and T. Hashimoto, "Thermal diffusivity of aromatic polyimide thin films by temperature wave analysis," J. Appl. Phys. **105**, 113506 (2009).
32. S. Tomonari, H. Yoshida, M. Kamakura, K. Yoshida, K. Kawahito, M. Saitoh, H. Kawada, S. Juodkazis, and H. Misawa, "Efficient microvalve driven by a Si-Ni bimorph," Jpn. J. Appl. Phys. **42**(part 1, No.7A), 4464–4468 (2003).
33. S. Tomonari, H. Yoshida, M. Kamakura, K. Yoshida, K. Kawahito, M. Saitoh, H. Kawada, S. Juodkazis, and H. Misawa, "Miniaturization of a thermally driven Ni|Si bimorph," Jpn. J. Appl. Phys. **42**(part 1, No.7A), 4593–4597 (2003).
34. R. Krishnan, S. Shirota, Y. Tanaka, and N. Nishiguchi, "High-efficient acoustic wave rectifier," Sol. State Comm. **144**, 194–197 (2007).
35. E. Gamaly, S.Juodkazis, V.Mizeikis, H. Misawa, A. Rode, and W. Krolokowski, "Modification of refractive index by a single fs-pulse confined inside a bulk of a photo-refractive crystal," Phys. Rev. B **81**, 054113 (2010).
36. S. Juodkazis, M. Sudzius, V. Mizeikis, H. Misawa, E. G. Gamaly, Y. Liu, O. A. Louchev, and K. Kitamura, "Three-dimensional recording by tightly focused femtosecond pulses in $LiNbO_3$," Appl. Phys. Lett. **89**, 062903 (2006).

#151731 - $15.00 USD Received 25 Jul 2011; revised 5 Sep 2011; accepted 5 Sep 2011; published 3 Oct 2011

1. Introduction

Non-contact optical methods are preferred in metrology and characterization of materials due to their versatility and simplicity. Thermal functioning of complex multi-component/layered structures in solar cells, MEMS and lab-on-a-chip applications should be well determined and controlled for new functions, enhanced performance, and monitoring of degradation. Creating and monitoring thermal distributions with a spatial resolution of $1-10$ μm is required in increasing number of applications [1–5], in particular, shunt regions of Si solar cells [6], evolution of hydrogen and oxygen and catalytic processes on TiO_2 surfaces [7]. Moreover, non-contact [6, 8] in situ and fast methods [9] have to be developed since the available contact methods [10–13], though precise and quantitative, cannot always be used, especially, in practical applications.

In the field of high precision three-dimensional (3D) laser fabrication effects of thermal and stress confinement should be better understood and monitored during structure formation. For example in 3D photo-polymerization [1, 3, 14] thermal curing of resins and resists can be used to achieve a 3D structuring by a 3D localized heat source of sub-micrometer dimensions [4, 15]. Thermal effects and heat affected zones (HAZ) should be well defined in laser dicing, scribing, and ablation [16] to control morphology and structural defects such as atom/ion interstitials and vacancies [17]. Similarly, thermal protocols and conditions have to be determined for the direct laser writing of waveguides and optical elements [2, 18–23], Marangoni or thermo-capillary flows in laser trapping [24–26], optofluidics [27], and thermoelectrical energy harvesting [28]. In situ monitoring of small, $\sim 1-10^{\circ}$C, temperature changes due to cooling or heating with the adequate temporal (defined by the cooling time of a heated spot < 10 ms) and spatial (smaller than the thermal diffusion length < 10 μm) resolutions are highly required for applications where temperature and its gradients are functional.

Here we show how temperature can be localized by patterns made using femtosecond (fs)-laser structuring inside polymer. The patterns of $\sim 20-50$ μm size can be used to create ~ 0.1 K/μm temperature gradients. Fs-laser structuring of the host polymer minimizes HAZ and degradation; the induced modifications are mostly of structural (mass density redistribution, void formation, polymer structure changes [29]) character rather than of a chemical nature. Small few percent changes of temperature diffusivity in the fs-structured regions were determined earlier by a miniaturized direct contact measurements [11–13, 29]. Here, we demonstrate an application of a non-contact thermal imaging with ~ 10 ms temporal, ~ 10 μm spatial, and ~ 0.1 $^{\circ}$C temperature resolution.

2. Experimental

2.1. Thermal imaging

Thermal imaging setup used in this study is shown in Fig. 1. The excitation source was a laser diode (LD) of 0.1 W power emitting at 630 nm wavelength. The optical pickup head was used to deliver light to inside/onto the sample by a PMMA lens of $D = 4$ mm diameter and f-number $f/\# = 1.0$. The corresponding numerical aperture was $NA = \frac{1}{2f/\#} = 0.5$ and the focal spot size on the sample is estimated to be $d = 1.22\lambda/NA \simeq 1.5$ μm. This is the size of a heat source in our experiments. Axial position of the heat source in the polymer film was optimized for maximum temperature increase on the surface under a IR-camera imaging.

A high-speed IR camera Phoenix (Indigo) and FLIR SC6000 having an indium-antimony (InSb) sensor array of 320×256 pixels and 640×512 pixels, respectively, with an optimum wavelength of operation between 3 and 5 μm, were used for taking a micro-scale thermography. The originally designed SiGe microscopic lens had a magnification of $7.5^{\times}$ and $8.3^{\times}$, respectively, with spatial resolution of 4.1×4.1 μm and 4.3×4.3 μm as calculated according to

#151731 - $15.00 USD Received 25 Jul 2011; revised 5 Sep 2011; accepted 5 Sep 2011; published 3 Oct 2011

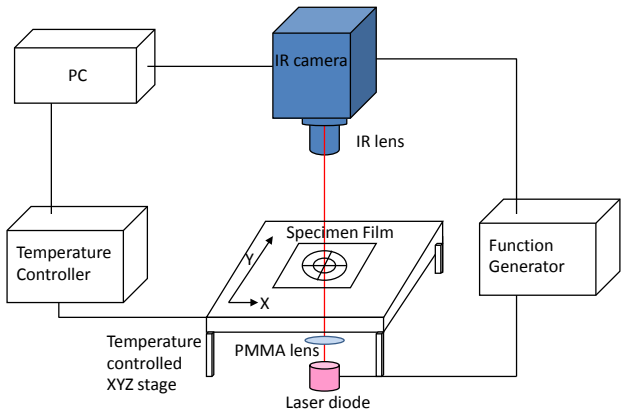

Fig. 1. Setup used for thermal imaging. Laser diode of 0.1 W power at 630 nm wavelength was used as a heat source; focusing was carried out by a lens of numerical aperture $NA = 0.5$. Data acquisition was performed on a personal computer (PC).

the NA of the used optics. The actual spatial resolution was tested with a standard USAF 1951 micro-scale. The image frame rate was selected between 60 and 120 frames/s. The photon count of the emitted intensity was detected with a 16 bit sensitivity.

Time differential images are calculated by standard procedure as $I'(t) = \frac{\partial I}{\partial t} = \lim_{\Delta t \to 0} \frac{I(t) - I(t-\Delta t)}{\Delta t}$, where $I(t)$ is the intensity at time moment t, Δt is time interval between the captured images. The Laplacian matrix was used in order to obtain the time differential image by selecting an optimum matrix size.

Digital Fourier transform (FT) was applied to obtain amplitude and phase of the thermal wave. The phase delay is calculated at each pixel with a locked reference of the modulated heat source. The calculated FT at each pixel $G(x,y) = A(x,y)e^{i\phi(x,y)}$ is further analyzed in terms of the amplitude $A(x,y)$ and phase, $\phi(x,y)$ maps.

Measurement of the absolute temperature increase, ΔT_{max}, (the amplitude) at the LD irradiation spot was carried out on a non-structured Kapton using a calibrated thermocouple. In all our experiments temperature jump was not exceeding 3°C at the center of illumination. The ΔT_{max} values at the fs-laser structured regions had comparable values, but were not calibrated since the emissivity of those regions depends on conditions of laser structuring (see discussion in the Sec. 3).

2.2. *Laser-structured patterns*

Patterns of void-structures were recorded inside the bulk of polymer films by direct laser writing using tightly focused fs-laser pulses. We used Kapton H (polyimide derived from pyromellitic dianhydride and 4,4'- oxydianiline (PMDA- ODA); Du Pont-Toray, Co., Ltd.) films of 75 μm thickness for fs-laser structuring under tighter ($NA = 1.42$) and less tight ($NA = 0.5$) focusing.

In the case of $NA = 1.42$, irradiated spots were placed in-plane (laterally) with separation of at least $dx, dy = 2 - 6$ μm (dx, dy is larger than the focal spot) in order to create voxels (volume elements) with central voids strictly at the one-per-pulse mode. The dimensions of the regions were filled with an opal-like arrangement of the void-structures and were $85_x - 85_y - 40_z$ μm^3 at pulse energy of 160 nJ (*region A*; the total number of pulses was $N = 3 \times 10^4$) and $75_x - 75_y - 40_z$ μm^3 with pulse energy of 200 nJ (*region B*; $N = 2.3 \times 10^4$). The energy is given at the entrance of the objective lens (the transmission of the objective lens was ~ 0.4).

In order to monitor a heat transport inside larger laser structured regions grating-like patterns

#151731 - $15.00 USD Received 25 Jul 2011; revised 5 Sep 2011; accepted 5 Sep 2011; published 3 Oct 2011

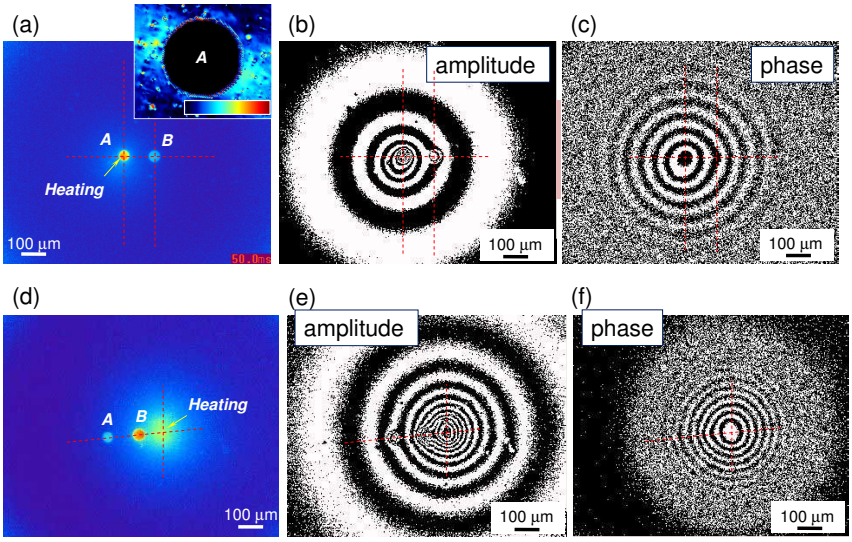

Fig. 2. (a-c) Thermal imaging of a heat wave in a 50-μm-thick Kapton film launched from the laser structured area shown in the inset polariscopy image; the inset color scale bar shows relative birefringence in a $1-247$ range. Amplitude (b) and phase (c) distributions. The cross-hair markers show centers of the 50-μm-diameter laser structured regions; the left-side region was illuminated by the LD to create heat wave and was modulated at 0.21 Hz frequency. The temperature amplitude was $\Delta T_{max} \simeq 2^{\circ}$C in unstructured Kapton (point *Heating* in (d)). (d-f) Same as (a-c) only with heating source placed outside the structured regions; modulation at 0.43 Hz. Regions *A*, *B* (in (a)) have been filled with opal-like arrangement of void-structures at 200 and 160 nJ per pulse, respectively (see, inset in (a)). Online video is available for (a) Media 1 and (d) Media 2.

were fabricated with period of 20 μm over area 760×760 μm^2, where central part of 120×140 μm^2 dimensions was left clear. Fabrication was performed using 800 nm wavelength 150 fs duration laser pulses focused by a $NA = 0.5$ objective. Three layers were stacked inside a 75-μm-thick Kapton film and placed at 20 μm inside from the top and bottom surfaces, the one above the other with a 15 μm vertical separation. Pulse energy was 280 nJ (at focus) and adjacent pulses were overlapping by approximately 95% of the focal spot diameter at the 100 μm/s scanning speed. These conditions of laser structuring are different from the used in the case of tight focusing where irradiation spots were separated. At the lower NA, the pulse power was ~ 1.9 MW/pulse indicating a presence of self-focusing. Structural modifications are dominated by melting and its fast quenching rather than void formation.

A spatial extent of temperature changes is determined by the temperature diffusivity of Kapton $\chi = (1.07 \pm 0.02) \times 10^{-7}$ m^{2}s^{-1} [11] and the LD's modulation frequency which was $f = 0.155 - 0.91$ Hz. Hence, the diffusion length $L_D = \sqrt{\chi \times \frac{1}{f}} \simeq 500 - 200$ μm in the thickness direction of the film; the diffusion coefficient along the surface plane is approximately twice larger as discussed in Sec. 3. The higher the repetition rate the smaller diffusion length and temperature modulation. At the used frequency, $1/f$ is much longer than the cooling time of the focal spot $t_c = d^2/\chi = 90$ μs; hence, no thermal accumulation occurred. The L_D and t_c are defining the adequate spatial and temporal resolutions of the experiments.

#151731 - $15.00 USD Received 25 Jul 2011; revised 5 Sep 2011; accepted 5 Sep 2011; published 3 Oct 2011

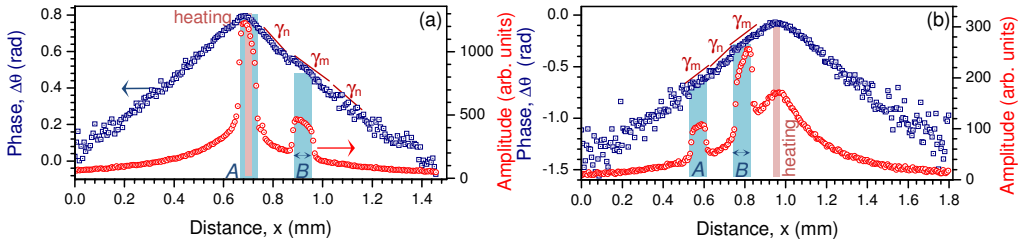

Fig. 3. Retrieved phase and amplitude cross sections when: (a) region *A* was heated (see, Fig. 1(a-c)) and (b) when heating was outside the laser structured area (Fig. 1(d-f)). Darker shade marks location of the heating source, the lighter shades show locations of laser-structured areas *A*, *B*; $\gamma_{m,n}$ marks the slope of phase, $\Delta\theta$, in the laser modified and unirradiated regions, respectively; $\Delta\theta$ is proportional to the temperature diffusivity.

3. Results and discussion

3.1. Closely-packed laser structured regions

For monitoring the transients of temperature distribution a heating point was located on the laser-structured region (Fig. 2(a-c)) or near it (Fig. 2(d-f)). The laser-structured region of 50-μm-diameter in Kapton is irradiated by a focused illumination of LD and creates a micrometer-sized heat source (a); see the online supplement video sequence. A spreading thermal wave was imaged and analyzed by FT with the amplitude and phase contour images shown in Fig. 2(b) and (c) panels, respectively. The entire laser structured region becomes the source of thermal wave whose spatial and temporal propagation beyond that region shows stronger localization and modulation amplitude as compared with the case where heating is adjacent to the laser structured areas (d-f). Temperature diffusivity is also affected by fs-laser structuring as can be seen by phase distribution contours (Fig. 2).

The FT amplitude is proportional to the emissivity ε of material and absolute temperature, T, according to the Stefan-Boltzmann law of a grey body emission: $j = \varepsilon\sigma T^4$, where j is the emissive power, σ is the Stefan-Boltzmann constant. The FT phase is linked to the temperature diffusivity χ and represents phase delay of the propagating heat wave.

Figure 3 shows the retrieved FT amplitude and phase profiles along the cross sections through the heat source and fs-laser structured areas for the data shown in Fig. 2. Change of the slope, γ, in the phase plot represents change of a temperature diffusivity, χ. The phase $\Delta\theta(x) = \sqrt{\frac{\omega}{2\chi}}x + Const$, where x is propagation coordinate and ω is the driving cyclic frequency of the heat source [30]. Decrease of the slope $\gamma \propto \sqrt{\frac{\omega}{2\chi}}$ signifies an increase of the χ value and vice versa. The laser structured regions showed larger thermal diffusivity (smaller slope, γ_m in Fig. 3) and confirmed our earlier observations by direct contact measurements. The increase of thermal diffusivity is consistent with void formation with air presence inside the film [11, 12].

The absolute temperature increase ΔT_{max} at the fs-laser structured regions cannot be directly determined since the emissivity ε of Kapton is dependent on conditions of laser fabrication. In the unstructured regions the maximum temperature increase at the same conditions were ~ 3°C. For the sake of estimation, let us assume that emissivity of fs-laser modified and unmodified regions is the same, $\varepsilon_m \simeq \varepsilon_n$, then the FT amplitude difference (see Fig. 3) of approximately 5 times would indicate the difference in ΔT_{max} on the order of $\sqrt[4]{5} \simeq 1.5$ times, i.e., $\Delta T_{max;m} = 1.5\Delta T_{max;n} \simeq 4.5$°C. This provides the upper bound of the expected temperature jump. Since the emissivity of laser structured regions has been slightly increased, as can be judged from a brighter appearance of the laser structured regions (see, the online material), the

#151731 - $15.00 USD Received 25 Jul 2011; revised 5 Sep 2011; accepted 5 Sep 2011; published 3 Oct 2011

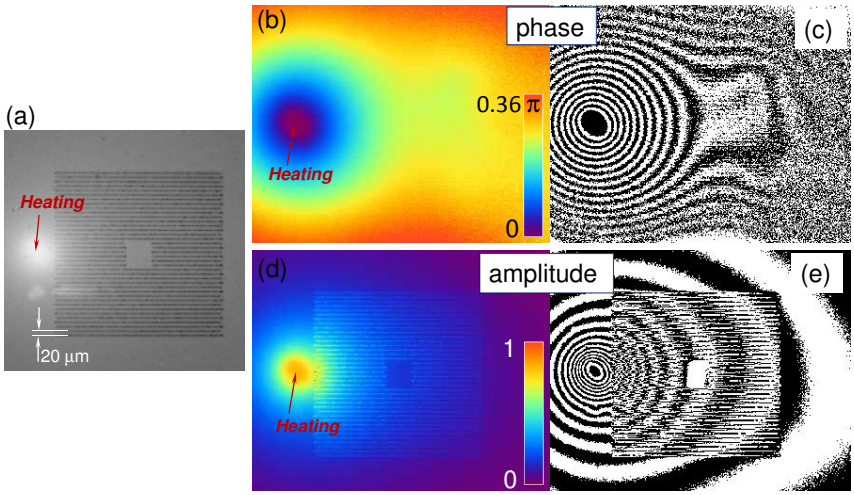

Fig. 4. Temperature wave; a stationary heat source. Localization of temperature and diffusion in laser-structured regions. (a) Thermo-image of a grating structure recorded in a 75-μm-thick PI-Kapton film by scanning 800 nm/150 fs laser pulses at three different depths separated by ~ 10 μm, which is approximately the axial length of modification; focusing was carried out by an objective lens of numerical aperture $NA = 0.5$. The phase $\Delta\theta \propto \sqrt{\frac{1}{2\chi}}$ (b-c) and amplitude $\propto \varepsilon T^4$ (d-e) images; equal phase (c) and amplitude (e) contour plots reveals more detailed features as compared to the FT data (b) and (d), respectively. Heat source was laser diode emitting at 630 nm and was modulated at 0.91 Hz. Online video is available for (a) Media 3.

actual temperature increase was smaller.

The difference between the slopes, γ, in laser modified and unirradiated regions was $\frac{\gamma_m-\gamma_n}{\gamma_n} \simeq 40\%$, here the experimentally determined values from the phase shift slope are $\chi_m = (5.4 \pm 0.1) \times 10^{-7}$ m^2/s and $\chi_n = (3.9 \pm 0.1) \times 10^{-7}$ m^2/s. The thermal diffusivity in the lateral direction is consistent with typically larger values as compared with those obtained by the direct contact measurements in the through-the-film direction [11, 12]. For example, the lateral diffusion coefficient of a 125-μm-thick Kapton was $\sim 3.8 \times 10^{-7}$ m^2/s and was by 36% smaller than in air as measured in a separate experiment. It can be partially explained by anisotropic thermal properties of polymer sheets made by extrusion [31]. In addition, a surface heat transport mediated by air, which has a much larger temperature diffusivity, $\chi_{air} = 2.1 \times 10^{-5}$ m^2/s [11], than the polymer can cause larger χ values determined by the IR monitoring. It is noteworthy that the temperature diffusivity measured by the non-contact IR imaging reflects the actual performance of the pattern in air, as it would be in some of applications. Hence, IR-imaging is a very appropriate technique and provides an effective χ value influenced by the air ambient.

Figures 2(a) and 3(a) show that laser structured regions localize temperature. The phase plots also show that temperature dissipation is affected by fs-structured regions. This provides a possibility to redirect heat flow on the surface on the scale of tens-of-micrometers. This is prospective in MEMS applications where the temperature should be controlled and localized to perform, e.g., a hydrogen valve function using bimorphs [32, 33]. In microscopy of living cells, thermal gradients of several degrees can be utilized to induce photo-phoretic forces, affect membranes, and laser trapping [25].

#151731 - $15.00 USD Received 25 Jul 2011; revised 5 Sep 2011; accepted 5 Sep 2011; published 3 Oct 2011

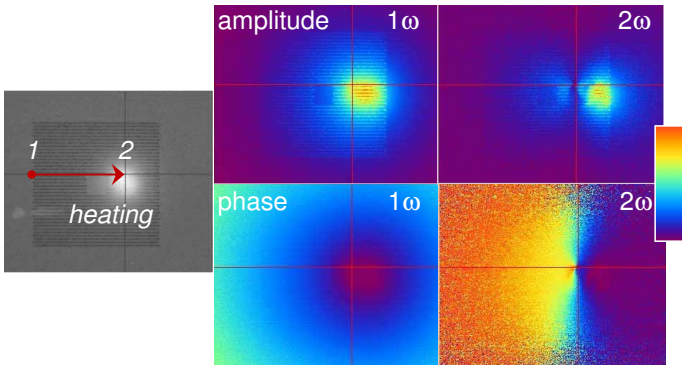

Fig. 5. Temperature wave; a moving heat source. The thermal image, its Fourier amplitude and phase at the fundamental driving frequency of LD $1\omega = 0.93$ Hz, and its second harmonics 2ω (the same sample as in the Fig. 4). Scale bar represents 0 - π span for the phase and 0 - 1 for the amplitude. Sample is scanned from the edge of the laser structured pattern (point *1*) along the structured region (along the arrow) at speed of 79.5 μm/s.

3.2. Towards to directional heat flow in laser-structured regions

To explore a wave character of the heat transport we used a grating-like structures with three fs-laser fabricated layers fabricated with large, 20 μm period (see, Fig. 4(a)). This pattern has induced an anisotropy in a heat flow. The FT analysis reveals a spatial control over the temperature and emissivity (amplitude) and heat propagation (phase) through out the laser fabricated micro-grating; it is noteworthy that emissivity changes might be slightly different as compared to the samples made at tight focusing (Fig. 2). Figure 4(c,e) represents the same data shown in panels (b,d) only in a contour plot fashion for the clearer presentation of the phase and amplitude maps. The central unstructured region caused a phase front planarization (c). The difference in temperature or/and emissivity in the laser structured vs. unstructured regions is obvious as a distortion and horizontal elongation of the contours shown in (e).

The same features observed in the case of small micro-structured volumes (Fig. 2) are collaborated on the sub-mm scale, namely, the fs-modified regions have different emissivity and ability to localize temperature changes. The diffusive heat transport can be controlled in terms of directionality using anisotropy of thermal properties preconditioned by fs-laser structuring similarly to the optical anisotropy induced by the form birefringence.

When heating spot was scanned over the grating region, a complex heat transport peculiarities were revealed by the FT analysis (Fig. 5) and can be rationalized by frequency beatings at the fundamental ω and 2ω frequencies existing in the signal driving the LD illumination. At the 2ω frequency, there was a stationary pattern of the amplitude and phase established, which corresponds to the temperature spreading over the laser structured region. The maximum of amplitude at 2ω was shifted from the actual irradiation point and can be explained by temperature diffusion and localization in the laser modified regions. The phase map, which is linked to the temperature diffusivity, shows that the maximum of the temperature was not localized at the irradiation spot and is consistent with anisotropy and localization in temperature propagation. It is noticeable that the spot of an augmented temperature/emissivity (Fig. 5) is elongated along the laser structured fringes of grating-structure and coincides with direction of the sample scan. Further experiments will be carried out to reveal details of heat propagation and its directionality control. Current observations confirm that a heat diffusion can be controlled by fs-laser structured regions.

A closeup analysis of the contour cross-sections of the phase in the central open window

#151731 - $15.00 USD Received 25 Jul 2011; revised 5 Sep 2011; accepted 5 Sep 2011; published 3 Oct 2011

(Fig. 4(e)) also collaborates a wave character of the heat transport. By creating locations where heat is localized, the heat transport can be controlled on a micro-scale. The observed increase of the FT amplitude is apparent and is caused by the emissivity change of laser structured polymer. The FT amplitude shows a boundary effect similar to optical Snells' law when heat diffuses through out the regions of different emissivity (laser structured and unstructured, Fig. 4). Anisotropy induced by fs-laser pulses can be used to control a diffusive heat transport on the scale comparable with the living cell size, $\sim 10\ \mu$m, at a video rate or faster, and small relative $\sim 0.1^{\circ}$C changes can be detected and in situ monitored.

4. Conclusions

Fs-laser structuring can be used to control heat transport on a micro-scale, at a video rate, and with high thermal sensitivity. Simultaneous spatial and temporal monitoring of temperature diffusivity is demonstrated using non-contact thermal imaging with sensitivity of $\sim 0.1^{\circ}$C. Small changes of thermal properties of fs-laser structured Kapton are reliably measured in a non-contact mode for the first time with high spatial, $\sim 10\ \mu$m, and temporal, ~ 10 ms, resolution.

It is revealed that fs-laser structured regions can be, in principle, used to create required patterns of temperature distribution and define its diffusion via engineering of thermal anisotropy similarly to the form birefringence in optics. One can envisage micro-structures which would have a diode-type functionality for the heat flow as already debated in literature [34]. Thermo-electrical conversion and energy harvesting [28] is another field where thermal conductivity can be controlled by defects introduced by fs-laser pulses as we demonstrated in lithium niobate where spatial charge distribution (and the corresponding refractive index modulation) where controlled on a micrometer scale by a laser direct write-erase cycling [35, 36].

Acknowledgments

We gratefully acknowledge a partial support of this work by JST (SENTAN, Development of System and Technology for Advanced Measurement and Analysis). SJ is grateful to Tokyo Institute of Technology for the research visit support.

#151731 - $15.00 USD Received 25 Jul 2011; revised 5 Sep 2011; accepted 5 Sep 2011; published 3 Oct 2011